






Article

# Motion-Based Design of Passive Damping Systems to Reduce Wind-Induced Vibrations of Stay Cables under Uncertainty Conditions

Javier Naranjo-Pérez <sup>1</sup>, Javier F. Jiménez-Alonso <sup>2,\*</sup>, Iván M. Díaz <sup>2</sup>, Giuseppe Quaranta <sup>3</sup> and Andrés Sáez <sup>1</sup>

<sup>1</sup> Department of Continuum Mechanics and Structural Analysis, Universidad de Sevilla, 41092 Seville, Spain; jnaranjo3@us.es (J.N.-P.); andres@us.es (A.S.)

<sup>2</sup> Department of Continuum Mechanics and Theory of Structures, E.T.S. Ingenieros de Caminos, Canales y Puertos, Universidad Politécnica de Madrid, 28040 Madrid, Spain; ivan.munoz@upm.es

<sup>3</sup> Department of Structural and Geotechnical Engineering, Sapienza University of Rome, 00184 Rome, Italy; giuseppe.quaranta@uniroma1.it

\* Correspondence: jf.jimenez@upm.es; Tel.: +34-910-674-152

Received: 31 December 2019; Accepted: 28 February 2020; Published: 3 March 2020



**Abstract:** Stay cables exhibit both great slenderness and low damping, which make them sensitive to resonant phenomena induced by the dynamic character of external actions. Furthermore, for these same reasons, their modal properties may vary significantly while in service due to the modification of the operational and environmental conditions. In order to cope with these two limitations, passive damping devices are usually installed at these structural systems. Robust design methods are thus mandatory in order to ensure the adequate behavior of the stay cables without compromising the budget of the passive control systems. To this end, a motion-based design method under uncertainty conditions is proposed and further implemented in this paper. In particular, the proposal focuses on the robust design of different passive damping devices when they are employed to control the response of stay cables under wind-induced vibrations. The proposed method transforms the design problem into a constrained multi-objective optimization problem, where the objective function is defined in terms of the characteristic parameters of the passive damping device, together with an inequality constraint aimed at guaranteeing the serviceability limit state of the structure. The performance of the proposed method was validated via its application to a benchmark structure with vibratory problems: The longest stay cable of the Alamillo bridge (Seville, Spain) was adopted for this purpose. Three different passive damping devices are considered herein, namely: (i) viscous; (ii) elastomeric; and (iii) frictions dampers. The results obtained by the proposed approach are analyzed and further compared with those provided by a conventional method adopted in the Standards. This comparison illustrates how the newly proposed method allows reduction of the cost of the three types of passive damping devices considered in this study without compromising the performance of the structure.

**Keywords:** motion-based design; uncertainty conditions; constrained multi-objective optimization; reliability analysis; passive structural control; cable-stayed bridges

## 1. Introduction

One of the main elements that governs the dynamic behavior of cable-stayed bridges is their stay cables [1]. This structural system has both a high flexibility and a low damping, which makes it susceptible to suffer both from different vibratory problems [2] and exhibit significant changes in its modal properties induced by the modification of the operational and environmental conditions [3].

The vibratory problems observed in cables of cable-stayed bridges may be classified in terms of the structural elements excited during the vibration phenomenon into the following [2]: (i) local-global vibratory problems, in which the vibrations involve the excitation of both the cables and the deck of the structure [4]; and (ii) local vibratory problems, in which only the cables of the structure are excited laterally [5]. These vibratory problems may be caused by either of the following: (i) direct excitation sources, such as road traffic, wind [6] or earthquake action [7], or (ii) indirect excitation sources, such as linear internal resonances, parametric excitations or dynamic bifurcations.

In this paper, we focus on the case of wind-induced vibrations of stay cables, as this is the source problem of many vibratory issues reported in the literature [2]. As wind-induced vibrations can cause different structural problems on stay cables (like fatigue or comfort problems), two types of measures are normally adopted to mitigate the cable vibrations [8], consisting of either of the following: (i) modifying its natural frequency via the installation of a secondary net of cables [9]; or (ii) increasing its damping ratio via the installation of external control systems [2]. Such control systems for stay cables may be classified into three different groups [8]: (i) active [10]; (ii) semi-active [11]; and (iii) passive [12].

Active control systems for stay cables focus on controlling the dynamic response of the cable via the modification of its tensional state [13]. For this purpose, some kind of actuator, following the orders of a controller, acts on the cable in order to minimize the difference between the actual response of the cable (recorded by a sensor) and the allowable response value [14]. Although the theoretical research on the use of these devices has experienced a significant growth in recent years, their practical implementation in real cable-stayed bridges has been limited due to their high cost and the robustness problems associated with the power supply needed to guarantee their operation [2].

On the other hand, semi-active control systems focus on modifying the constitutive parameters of external damping devices deployed to control the response of the stay cable under external actions [15]. Among the different semi-active devices, magnetorheological dampers have been widely studied and implemented in real cable-stayed bridges [16]. Although semi-active damping devices outperform their passive damping counterparts [17] with a lower cost than active control systems, their efficiency is limited when they are employed under uncertainty conditions, since their performance highly depends on the control algorithm considered for the design [18].

Finally, passive control systems for stay cables focus on increasing the damping ratio of the cables via the installation of external devices, whose characteristic parameters are originally designed to mitigate the dynamic response of the structural system [19]. Due to the robustness of such passive damping devices [20], they have been installed successfully on numerous real cable-stayed bridges to reduce wind-induced vibrations [21]. Nevertheless, these devices present as main limitation, a lower flexibility to adapt the system response to the variability of both the external actions and the modification of the stay cable parameters induced by loading, when compared to the active and semi-active devices. In order to overcome this limitation, two strategies may be adopted as outlined: either (i) to install a hybrid control system [22]; or (ii) to design the passive damping device taking into account these uncertainty conditions via a robust design method [23].

Different design methods have been developed for this purpose. Among the different proposals, Kovacs was the first researcher to study the optimum design of viscous dampers for stay cables [24]. Subsequently, Pacheco et al. provided a universal curve which allows the representation of the modal damping of the first vibration mode of a taut cable in terms of the damping coefficient of the viscous damper [25]. The maximum of this curve corresponds to the optimum damping ratio of the taut cable when a viscous damper is installed on it. Later, Krenk et al. obtained an analytical expression for this curve [26]. Alternatively, other authors, such as Yoneda and Maeda, proposed an analytical model of the damped cable to determine the optimum parameters of the passive damper [27]. Although the design parameters obtained following any of these approaches are similar, so that they are currently employed for the practical design of passive damping devices, they fail to take into account a key aspect: the uncertainty associated with the variation of both the external actions and the modification of the modal properties of the stay cables [28].

In order to overcome this limitation, a motion-based design method [29] under uncertainty conditions is formulated, implemented and further validated in this paper. In fact, this proposal generalizes the formulation of a well-known design method, the so-called motion-based design method under deterministic conditions [30], to the abovementioned uncertainty conditions. The proposed motion-based design method under uncertainty conditions transforms the design problem into a constraint multi-objective optimization problem. Hence, the main objective of this problem is to find the optimum values of the characteristic parameters of the passive damping device which meet the design requirements for the structure. For this purpose, a multi-objective function is defined in terms of these parameters, together with an inequality constraint aimed at guaranteeing the compliance of the design requirements. Such design requirements are defined in terms of the vibration serviceability limit state of the structure. Since this serviceability limit state is defined under stochastic conditions, the failure probability of its compliance must be limited [31] and a reliability analysis must be performed [32,33]. For practical engineering applications [34], an equivalent reliability index is usually considered instead of the probability of failure. Thus, the formulation of the inequality constraint is realized in terms of the reliability index, which cannot exceed an allowable value [35]. For the computation of the reliability index, a sampling technique, the Monte Carlo method has been considered herein [36].

Finally, in order to validate the performance of the proposed method, it was applied to the robust design of three different passive damping devices (viscous, elastomeric, and friction dampers) where they are installed on the longest stay cable of the Alamillo bridge (Seville, Spain). To this end, only the effect of the rain–wind interaction phenomenon and the turbulent component of the wind action were considered. The results were compared with those obtained applying a conventional approach. This comparative study reveals that the proposed method allows the reduction of the cost of the passive damping devices while ensuring the structural reliability of the stay cable.

The manuscript is organized as follows: First, the motion-based design method under uncertainty conditions is described in detail. Next, a damper-cable interaction model under wind action, based on the finite element (FE) method, is presented. Subsequently, the performance of the proposed method is illustrated and further validated with a case-study (Alamillo bridge, Seville, Spain). In the final section, some concluding remarks are drawn to complete the paper.

## 2. Motion-Based Design of Structures under Uncertainty Conditions

### 2.1. Motion-Based Design of Structures under Deterministic Conditions

Structural optimization is a computational tool which can be used to assist engineering practitioners in the design of current structural systems [37]. Thus, this computational tool allows the optimum size, shape or topology of the structure to be found which meet the design requirements established by the designer/manufacturer/owner. Among the different structural optimization methods, the performance-based design method has been widely employed to design passive damping devices for civil engineering structures [23,30]. When the design requirements are defined in terms of the vibration serviceability limit state of the structure, the performance-based design method is denominated the motion-based design method [29]. This general design method was adapted herein for the design of passive damping devices when they are used to control the dynamic response of civil engineering structures. As assumption, all the variables, involved in this problem, are deterministic.

Thus, the motion-based design method under deterministic conditions transforms the design problem into a constrained multi-objective optimization problem. Therefore, the main objective of this problem is to find the optimum value of the characteristic parameters of the passive damping devices which guarantee an adequate serviceability structural behavior. For this purpose, a multi-objective function is minimized. The multi-objective function,  $f(\theta)$ , is defined in terms of the characteristic parameters,  $\theta$ , of the considered passive damping devices. Additionally, the space domain is constrained including two restrictions in the optimization problem: (i) an inequality constraint,  $g_{det}(\theta)$ ; and (ii) a search domain.  $[\theta_{min}, \theta_{max}]$ . As the relation between the objective function and the design

variables is nonlinear, global optimization algorithms are normally considered to solve this constrained multi-objective optimization problem. [38]. Accordingly, the motion-based design problem under deterministic conditions can be formulated as follows:

$$\begin{aligned} & \text{Find } \boldsymbol{\theta} \text{ to Minimize } f(\boldsymbol{\theta}) \\ & \text{Subjected to } \begin{cases} g_{det}(\boldsymbol{\theta}) \leq 0 \\ \boldsymbol{\theta}_{min} < \boldsymbol{\theta} < \boldsymbol{\theta}_{max} \end{cases} \end{aligned} \tag{1}$$

where  $\boldsymbol{\theta}$  is the vector of the design variables;  $f(\boldsymbol{\theta})$  is the multi-objective function to be minimized;  $\boldsymbol{\theta}_{min}$  and  $\boldsymbol{\theta}_{max}$  are the lower and upper bounds of the search domain; and  $g_{det}(\boldsymbol{\theta})$  is a function which defines the inequality constraint.

Therefore, the key aspect of this optimization problem is the definition of the inequality constraint. In the case of slender civil engineering structures, whose design is conditioned by their dynamic response [29], the compliance of the vibration serviceability limit state can be considered for this purpose. According to the most advanced design guidelines [6,34], the vibration serviceability limit state of a structure is met if the movement of the structure,  $d_s(\boldsymbol{\theta})$ , which can be characterized by its displacement, velocity or acceleration, is lower than an allowable value,  $d_{lim}$ , defined in terms of the considered comfort requirements. Thus, the inequality constraint of the abovementioned optimization problem may be expressed as follows:

$$g_{det}(\boldsymbol{\theta}) = \frac{d_s(\boldsymbol{\theta})}{d_{lim}} - 1 \leq 0 \tag{2}$$

Finally, as the result of this multi-objective optimization process, a set of possible solutions is obtained. This set of possible solutions is denominated the Pareto front. Accordingly, a subsequent decision-making problem must be solved, the selection of the best solution among the different elements of this Pareto front. Two possible alternatives are normally considered for this purpose [23]: (i) the selection of the best-balanced solution among all the elements of the Pareto front; and (ii) the consideration of additional requirements to solve this decision-making problem. The selection between both alternatives depends on the designer’s own criterion and the particular conditions of the problem.

### 2.2. Motion-Based Design of Structures under Stochastic Conditions

In order to generalize the implementation of the motion-based design method to scenarios with stochastic conditions, it is necessary to consider during the design process the uncertainty associated with the variability of both the external actions and the modal properties of the structure. For this purpose, two types of methods are normally employed [33]: (i) probabilistic methods; and (ii) fuzzy logic methods. Between these two methods, a probabilistic approach was considered herein because engineering practitioners are more used to dealing with probability concepts than with fuzzy logic problems. Concretely, a structural reliability method [39] was adapted herein to deal with the aforementioned uncertainty. According to this method, the vibration serviceability limit state can be expressed as a probabilistic density function,  $g_{unc}(\boldsymbol{\theta})$ , which is defined in terms of the capacity of the structure,  $C_s$ , and the demand of the external actions,  $D_a(\boldsymbol{\theta})$  (where both terms are random variables characterized by their probability density function). Thus, the vibration serviceability limit state can be defined as follows:

$$g_{unc}(\boldsymbol{\theta}) = \begin{cases} C_s - D_a(\boldsymbol{\theta}) & \text{if } g_{unc}(\boldsymbol{\theta}) \text{ is assumed normally distributed} \\ \frac{C_s}{D_a(\boldsymbol{\theta})} & \text{if } g_{unc}(\boldsymbol{\theta}) \text{ is assumed log - normally distributed} \end{cases} \tag{3}$$

The above relation (Equation (3)) allows the computation of the probability of failure of the structural system,  $p_f(\theta)$ , to the vibration serviceability limit state. This probability of failure,  $p_f(\theta)$ , may be determined as follows:

$$p_f(\theta) = \begin{cases} \text{Prob}[g_{unc}(\theta) < 0] & \text{if } g_{unc}(\theta) \text{ is assumed normally distributed} \\ \text{Prob}[g_{unc}(\theta) < 1] & \text{if } g_{unc}(\theta) \text{ is assumed log - normally distributed} \end{cases} \quad (4)$$

On the other hand, as it is shown in Figure 1, it is possible to characterize the probability of failure,  $p_f(\theta)$ , via an equivalent index, the so-called reliability index,  $\beta_s(\theta)$ .

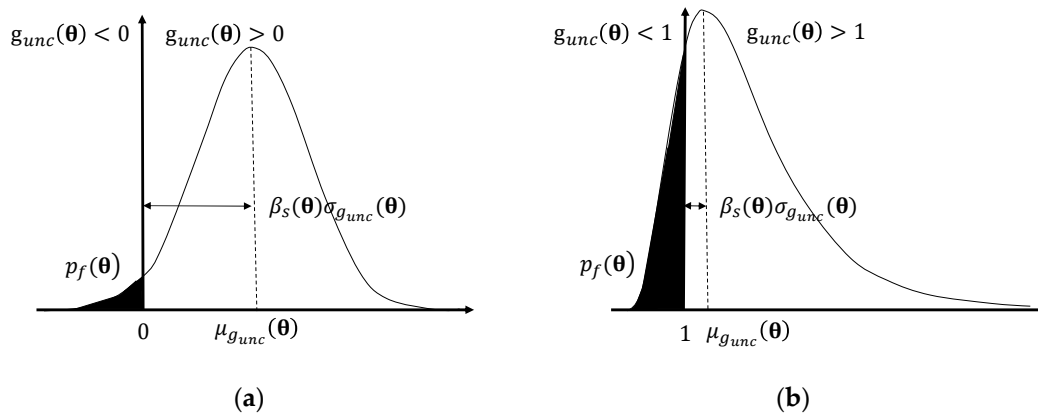


**Figure 1.** Probability density function of the vibration serviceability limit state,  $g_{unc}(\theta)$ : (a)  $g_{unc}(\theta)$  follows a normal distribution; and (b)  $g_{unc}(\theta)$  follows a log-normal distribution.

The relation between the probability of failure,  $p_f(\theta)$ , and the reliability index,  $\beta_s(\theta)$ , may be expressed as follows:

$$p_f(\theta) = \begin{cases} F_{g_{unc}}(0) = \Phi\left(-\frac{\mu_{g_{unc}(\theta)}}{\sigma_{g_{unc}(\theta)}}\right) = \Phi(-\beta_s(\theta)) & \text{normally distributed} \\ F_{g_{unc}}(1) = \Phi\left(\frac{\ln \mu_{C_s} / \mu_{D_a}(\theta)}{\sqrt{\sigma_{\ln C_s}^2 + \sigma_{\ln D_a}^2(\theta)}}\right) = \Phi(-\beta_s(\theta)) & \text{log - normally distributed} \end{cases} \quad (5)$$

where  $F_{g_{unc}}$  is the cumulative probability distribution function of  $g_{unc}(\theta)$ ;  $\mu_{g_{unc}(\theta)}$  and  $\sigma_{g_{unc}(\theta)}$  are respectively the mean and standard deviation of  $g_{unc}(\theta)$ ;  $\Phi$  is the standard normal cumulative distribution function;  $\mu_{C_s}$  and  $\mu_{D_a}(\theta)$  are respectively the mean of the probabilistic distribution function of  $C_s$  and  $D_a(\theta)$ ; and  $\sigma_{\ln C_s}$  and  $\sigma_{\ln D_a}(\theta)$  are respectively the standard deviation of the log-normal distribution of  $C_s$  and  $D_a(\theta)$ .

In this manner, the use of the reliability index,  $\beta_s(\theta)$ , allows the computation of the vibration serviceability limit state under uncertainty conditions to be simplified. Hence, this design requirement is met if the reliability index,  $\beta_s(\theta)$ , is greater than the allowable reliability index,  $\beta_t$ , established by the designer/manufacturer/owner of the structure. In order to evaluate this inequality constraints, the reliability index,  $\beta_s(\theta)$ , is usually computed via sampling techniques and the recommended values of the allowable reliability index,  $\beta_t$ , can be found in literature [39]. In this study, Monte Carlo simulations [36] were considered in order to evaluate numerically the reliability index,  $\beta_s(\theta)$ , and the value proposed by the European guidelines [34] was considered for the allowable reliability index,  $\beta_t$ .

Finally, the motion-based design method under uncertainty conditions may be formulated as follows:

$$\begin{aligned} & \text{Find } \theta \text{ Minimize } f(\theta) \\ & \text{Subjected to } \begin{cases} g_{unc}(\theta) = \frac{\beta_t}{\beta_s(\theta)} - 1 \leq 0 \\ \theta_{\min} < \theta < \theta_{\max} \end{cases} \end{aligned} \quad (6)$$

According to this, one of the main virtues of the motion-based design method is highlighted. The method allows the deterministic and stochastic design problems to be dealt with using a similar formulation. Only the inequality constraint must be modified to adapt the formulation to the particular conditions of each problem. This virtue facilitates the implementation of this method for the robust design of passive damping devices when they are used to control the dynamic response of slender civil engineering structures.

### 3. Damper-Cable Interaction Model under Wind Action

The damper-cable interaction model, considered herein to evaluate the dynamic response of a stay cable damped by different passive control systems under wind action, is described in detail in this section. First, the interaction model based on the FE method is introduced. Later, the method employed to simulate the wind action is presented.

#### 3.1. Modelling the Damper-Cable Interaction

The analysis of the dynamic behavior of stay cables has been studied extensively over the last four decades. Thus, analytical [40], numerical [30], and experimental studies [41] have been performed for this purpose. Among the different proposals, a numerical method, the FE method was considered herein to develop a damper-cable interaction model. This method presents three main advantages when it is implemented for this particular problem [30]: (i) its easy implementation for practical civil engineering applications; (ii) it allows a direct interaction of element with different constitutive laws (cable and dampers); and (iii) it simplifies the simulation of some effects such as the nonlinear behavior of the cable [40], the sag effect [42], and the influence of the external dampers on the modal properties of the cables (locking effect) [43].

The implementation of the FE method for this particular problem is based on the numerical integration of the weak formulation of the differential equilibrium equation of a vibrating stay cable in the lateral direction. Figure 2 shows an inclined cable of length,  $L$  [m], suspended between two supports at different level which presents a sag,  $d_c$  [m], with respect to the axis aligned with the two supports. The application of a small displacement causes the motion of a generic point from the self-weight configuration,  $P$ , to,  $P'$ , where  $u_c$  and  $v_c$  represent the component of the movement of the cable respectively in the parallel and perpendicular direction to the axis traced between the two supports. The equation, which governs the vibration of a taut cable in the lateral direction under the assumptions of linear and flexible behavior, may be expressed as follows:

$$H \frac{\partial^2 v_c}{\partial x^2} - \frac{\partial^2}{\partial x^2} \left( EI \frac{\partial^2 v_c}{\partial x^2} \right) = m \frac{\partial^2 v_c}{\partial t^2} \quad (7)$$

where  $v_c$  is the lateral displacement of the cable [m];  $H$  is the axial force of the cable [N];  $EI$  is the bending stiffness of the cable [ $\text{Nm}^2$ ] (where  $E$  is the Young's modulus [ $\text{N/m}^2$ ] and  $I$  is the moment of inertia of the cross-section of the cable [ $\text{m}^4$ ]); and  $m$  is the mass per unit length of the cable [ $\text{kg/m}$ ]. According to the Equation (7), the vibration of the cable is governed by both its tensional state and its bending stiffness [44,45]. Additional phenomena can be simulated via the selection of the adequate finite-element. A nonlinear two-node element with six degrees of freedom per node has been considered herein to simulate the cable behavior. This element allows both the nonlinear geometrical and stress-stiffness behavior of the cable to be simulated adequately [46].

In order to take into account, the initial tensional and deformational state of a stay cable during either a modal or a transient analysis, a preliminary static nonlinear analysis must be performed. In this preliminary static analysis, the equilibrium form of the cable under its self-weight and a preliminary axial force is achieved. As a result of this analysis, both the stress and the shape of the cable are updated, which is a key aspect to simulate numerically its real behavior.



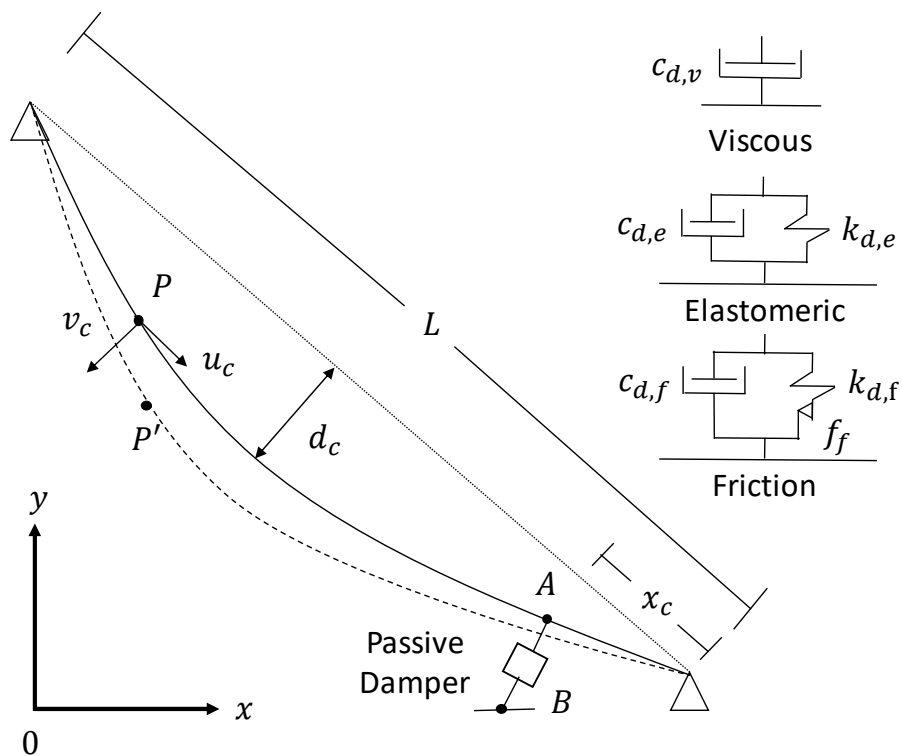


**Figure 2.** Damper-cable interaction model considered and mechanical model of each passive damper (viscous, elastomeric, and friction).

Subsequently, the modelling problem must focus on the simulation on the passive damping devices behavior. Three passive damping devices were considered herein (Figure 2). For these three passive damping devices, a linear constitutive law was assumed. The effect of these three passive damping devices on the cable may be simulated by an equivalent damping force. Each equivalent damping force is related to the energy that each damping device is able to dissipate, and it is opposed to the movement of the cable. Thus, each passive damping device has been modelled by a finite element whose behavior is equivalent to the corresponding damping force (Figure 2). This assumption has two advantages: (i) the relative movements between the damper and the cable, which govern the behavior of the damper, were obtained straight; and (ii) the effect of the dampers on the modal properties of the structure was taken into account directly.

First, the effect of a viscous damper is equivalent to a damping force which is proportional to a damping coefficient,  $c_{d,v}$  [sN/m], and the relative velocity,  $\dot{v}_r(t)$  [m/s], between the two extremes of the damper ( $\dot{v}_r(t) = \dot{v}_{d,A}(t) - \dot{v}_{d,B}(t)$ , where  $\dot{v}_{d,A}(t)$  is the velocity of the extreme of the damper in contact with the cable and  $\dot{v}_{d,B}(t)$  is the velocity of the extreme of the damper in contact with the deck, as it is illustrated in Figure 2. The viscous damping force of this damper,  $F_{d,v}(t)$ , may be expressed as [47]:

$$F_{d,v}(t) = c_{d,v} \dot{v}_r(t) \tag{8}$$

Second, the effect of the elastomeric damper may be simulated via the Kelvin–Voigt model. The equivalent viscoelastic damping force is characterized by two components: (i) a viscous damping component which is expressed in terms of a damping coefficient,  $c_{d,e}$  [sN/m], and the relative velocity,  $\dot{v}_r(t)$  [m/s]; and (ii) an elastic component which is expressed in terms of a stiffness coefficient,  $k_{d,e}$  [N/m], and the relative displacement between the two extremes,  $v_r(t)$  [m] ( $v_r(t) = v_{d,A}(t) - v_{d,B}(t)$ , where  $v_{d,A}(t)$  is the displacement of the extreme of the damper in contact with the cable and  $v_{d,B}(t)$  is the

displacement of the extreme of the damper in contact with the deck, as it is illustrated in Figure 2. The viscoelastic damping force of this damper may be defined as [48,49]:

$$F_{d,e}(t) = c_{d,e}\dot{v}_r(t) + k_{d,e}v_r(t) \tag{9}$$

Finally, the effect of the friction damper may be mimicked via the extended Kelvin–Voigt model. The definition of the equivalent damping force involves three components: (i) a viscous damping component which is expressed in terms of a damping coefficient,  $c_{d,f}$  [sN/m], and the relative velocity,  $\dot{v}_r(t)$  [m/s]; (ii) an elastic component which is expressed in terms of a stiffness coefficient,  $k_{d,f}$  [N/m], and the relative displacement,  $v_r(t)$  [m], and (iii) a friction component defined in terms of a static friction force,  $f_f$  [N] (where,  $f_f = \mu \cdot N$ , being  $\mu$  the friction coefficient [–] and  $N$  the normal force [N]) and a symbolic function,  $\text{sgn}(\dot{v}_r(t))$  (which returns –1, 0, and 1 in case  $\dot{v}_r(t) < 0$ ,  $\dot{v}_r(t) = 0$  and  $\dot{v}_r(t) > 0$ , respectively). The equivalent damping force of this damper may be expressed as [50]:

$$F_{d,f}(t) = c_{d,f}\dot{v}_r(t) + k_{d,f}v_r(t) + f_f \cdot \text{sgn}(\dot{v}_r(t)) \tag{10}$$

These damping devices are usually located at a certain distance,  $x_c$  [m], of the lower anchorage of the stay cable (Figure 2) due to constructive limitations. Nevertheless, due to their mechanical characteristics, they can have influence on both the damping and the natural frequencies (locking effect) of the stay cable.

### 3.2. Modelling the Wind Action

Subsequently, the effect of the wind-induced forces was simulated numerically. The wind simulation was carried out under the assumption that the cable is a cylinder immersed in a turbulent flow [2]. Hence, the wind flow is composed of three components: (i) a mean wind velocity,  $\mathcal{U}$  [m/s]; (ii) a fluctuating longitudinal velocity,  $u(t)$  [m/s]; and (iii) a fluctuating transversal velocity,  $v(t)$  [m/s].

The wind forces can be decomposed into a mean and a fluctuating component assuming the following hypothesis: (i) a quasi-steady behavior of the wind-induced forces; and (ii) small components of the turbulence with respect to the mean wind velocity,  $\mathcal{U}$  [51]. The expression of these two components can be expressed as follows (assuming a linearized approximation [52]):

$$F_D(t) = F_D + f_{Du}(t) + f_{Dv}(t) \tag{11}$$

$$F_L(t) = F_L + f_{Lu}(t) + f_{Lv}(t) \tag{12}$$

where  $F_D(t)$  is the drag force [N];  $F_L(t)$  is the lift force [N];  $F_D$  is the mean wind drag force;  $F_L$  is the mean wind lift force;  $f_{Du}(t)$  is the drag force induced by the longitudinal component of the wind;  $f_{Lu}(t)$  is the lift force induced by the longitudinal component of wind;  $f_{Dv}(t)$  is the drag force induced by the transversal component of wind; and  $f_{Lv}(t)$  is the lift force induced by the transversal component of the wind. These magnitudes can be determined using the following relationships [2]:

$$F_D = 0.5\rho\mathcal{U}^2DC_D \tag{13}$$

$$f_{Du}(t) = \rho\mathcal{U}u(t)DC_D \tag{14}$$

$$f_{Dv}(t) = 0.5\rho\mathcal{U}v(t)D(C'_D - C_L) \tag{15}$$

$$F_L = 0.5\rho\mathcal{U}^2DC_L \tag{16}$$

$$f_{Lu}(t) = \rho\mathcal{U}u(t)DC_L \tag{17}$$

$$f_{Lv}(t) = 0.5\rho\mathcal{U}v(t)D(C_L - C'_D) \tag{18}$$



where  $\rho$  is the density of the air [ $\text{kg/m}^3$ ];  $D$  is the outer diameter of the cable [m];  $C_D$  is the drag coefficient [-]; and  $C_L$  the lift coefficient [-]. The coefficients  $C'_D$  and  $C'_L$  are the derivative of  $C_D$  and  $C_L$ , respectively, with respect to the angle  $\alpha$  neighboring  $\beta$  (Figure 3). As the section of the cable is assumed to be circular in this study, these derivatives are therefore null because of the symmetry, and hence these two coefficients can be neglected.

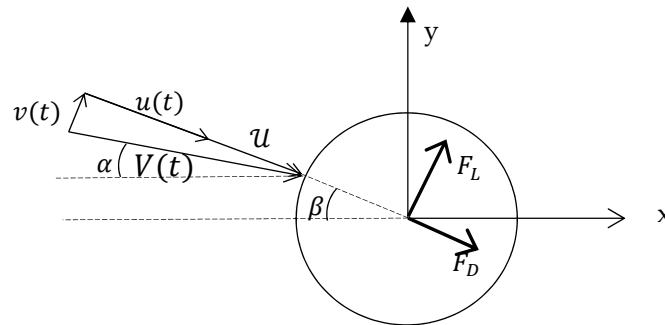


**Figure 3.** Reference coordinate system, drag force component, lift force component, and wind velocity components.

Finally, in order to determine the wind forces it is necessary to generate simulations of wind velocities. For this purpose, the wave superposition spectral-based method was considered [8]. This method allows the numerical determination of a series of wind velocities via the superposition of trigonometric functions. On the one hand, the amplitude of these functions is obtained in terms of a coherence function, which considers the spatial variability of the wind velocity, and the power spectral density function of the turbulent wind velocity. On the other hand, the phase of the trigonometric functions is generated randomly. The coherence function is defined using the relationship proposed by Davenport [53]. The power spectral density function proposed by the European guidelines [54] was considered herein.

#### 4. Application Example

The proposed motion-based design method under uncertainty conditions was validated herein via the design of three passive damping devices when they are used to control the wind-induced vibrations of the longest cable of a real bridge. For this purpose, the Alamillo bridge (Seville, Spain) was considered (Figure 4). The length of the deck of this bridge is 200 m. Unlike most cable-stayed bridges, the Alamillo bridge has not back-stays. An inclination of its pylon of  $32^\circ$  with respect to the vertical axis compensates the lack of the back-stays [55]. A total of 26 stays (13 parallel pairs) with a longitudinal separation of 12 m guarantees an adequate connection between the deck and the pylon.

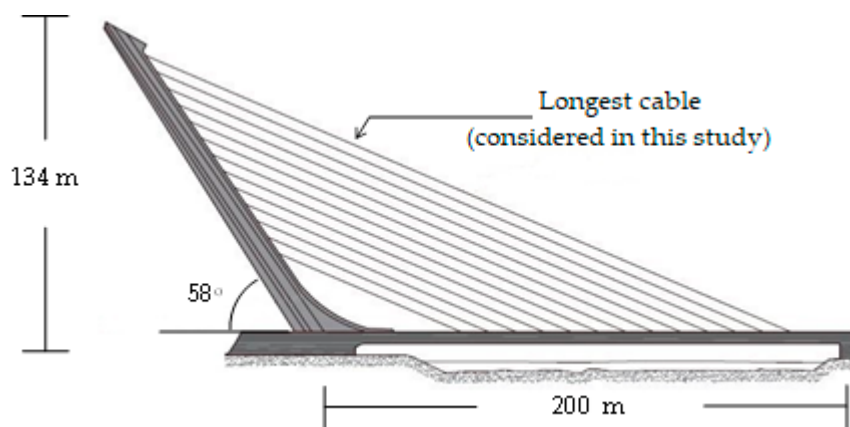


**Figure 4.** Illustrative scheme of the Alamillo bridge.

Previous research reported that the longest stay cable of this bridge, which has both a low damping and mass ratio, was prone to vibrate due to the wind action. Concretely, it was detected that the main sources of vibration of this cable were the rain–wind interaction phenomenon and the turbulent component of the wind action [56]. Therefore, this stay cable was considered as a benchmark to validate the performance of the proposed design method. For this purpose, three different passive damping devices (viscous, elastomeric and friction dampers) were designed according to the proposed method, and the results obtained were compared with the ones provided by a conventional method adopted by the Standards [6]. Additionally, the uncertainty associated with the variation of the modal properties of the cable due to the modifications of the operational and environmental conditions was taken into account in this design process. The development of this case-study was organized in the following steps: (i) a FE model of the cable was built and its numerical modal properties were obtained via a numerical modal analysis; (ii) a transient analysis was performed to evaluate the vibration serviceability limit state of the structure; (iii) as this limit state was not met, the three passive damping devices were designed according to both methods (the new proposal and the conventional one); and (iv) finally, the results obtained were compared and some conclusions were drawn to close the section.

#### 4.1. FE Model and Numerical Modal Analysis

The FE model of the cable was built using the software Ansys [57]. The geometrical and mechanical properties of the cable under study were as follows: (i) its length,  $L = 2.92 \times 10^2$  m; (ii) its outer diameter,  $D = 0.20$  m; (iii) the effective area of its cross section,  $A = 8.38 \times 10^{-3}$  m<sup>2</sup>; (iv) the effective moment of inertia,  $I = 5.58 \times 10^{-4}$  m<sup>4</sup>; (v) its mass per unit length,  $m = 60$  kg/m; (vi) an axial force,  $H = 4.13 \times 10^6$  N; (vii) a Young's modulus,  $E = 1.6 \times 10^{11}$  N/m<sup>2</sup>; and (viii) the angle between the cable and the deck,  $\gamma = 26^\circ$ . The cable was modelled by a mesh of 100 equal-length beam elements (BEAM188). In order to simulate numerically the sag effect, a nonlinear static analysis was previously performed. The objective of this preliminary analysis was to find both the initial tensional state and pre-deformed shape of the cable. The self-weight of the cable and its initial axial force were considered as loads for this preliminary nonlinear static analysis. Subsequently, the results of this analysis were used to update the geometry and tensional state of the cable. Later, the linear perturbation method was considered to perform the modal analysis [57]. Additionally, the stress stiffening effect was taken into account to perform this modal analysis.

As result of this numerical modal analysis, the first six natural frequencies were obtained. Table 1 shows the value of these first six natural frequencies ( $f_i$  being the natural frequencies of the  $i^{th}$  vibration mode).

**Table 1.** Numerical natural frequencies of the cable.

Natural Frequency	$f_1$	$f_2$	$f_3$	$f_4$	$f_5$	$f_6$
Value [Hz]	0.452	0.905	1.351	1.802	2.254	2.706

#### 4.2. Assessment of the Vibration Serviceability Limit State of the Cable under Uncertainty Conditions

As it was expected, according to the numerical natural frequencies obtained (Table 1), this cable was prone to vibrate under wind action due to both the turbulent component of the wind (the first two natural frequencies are lower than 1 Hz [58]) and the rain–wind interaction phenomenon (the six natural frequencies are lower than 3 Hz [6]). For this reason, the assessment of the vibration serviceability limit state of this stay cable was performed herein following the recommendations of the Federal Highway Administration (FHWA) guidelines [6].

On the one hand, in order to avoid the wind-induced vibrations associated with the rain–wind interaction phenomenon, it must be checked that the damping ratio of all the vibration modes, whose natural frequencies are lower than 3 Hz, are greater than a recommended value [6,59]. In order to determine this recommended value, the FHWA guidelines [6] establishes that the rain–wind interaction

phenomenon can be neglected if the Scruton number,  $S_c$ , is greater than 10 for all the considered vibration modes. This condition may be expressed as follows:

$$S_{c,i} = \frac{m\xi_i}{\rho D^2} > 10 \tag{19}$$

where  $\xi_i$  is the damping ratio of the  $i^{th}$  vibration mode.

Thus, this requirement is equivalent to guaranteeing a minimum damping ratio for each considered vibration mode. The minimum required damping ratio may be determined as follows:

$$\xi_i > \frac{10\rho D^2}{m} \tag{20}$$

As expected, due to the results of previous experimental tests, the damping ratio associated with the first six vibration modes of this cable did not meet this condition [56]. Hence, it was necessary to increase the value of these damping ratios. A passive damping device can be designed and installed on the cable for this purpose.

On the other hand, in order to analyze the effect of the turbulent component of wind action on the dynamic behavior of the cable, a transient analysis was performed. As a result of this transient analysis, the dynamic response of the cable under wind action can be obtained and the vibration serviceability limit state of the cable can be assessed. According to the FHWA guidelines [6], this limit state is met if the maximum displacement of the cable is lower than an allowable displacement which is defined in terms of the user tolerance. Table 2 shows the allowable displacement of the cable in terms of the design level required [6]. In this study, a recommended design level was established for the vibration serviceability limit state.

**Table 2.** User tolerance limits for the different design levels [6].

Design Level	Allowable Displacement [m] <sup>1</sup>
preferred	0.5D
recommended	1.0D
not to exceed	2.0D

<sup>1</sup> D is the outer diameter of the cable.

Additionally, as the dynamic response of the stay cable was sensitive to the variation of its modal properties associated with the change of the operational and environmental conditions during its overall life cycle, a reliability analysis about the compliance of the vibration serviceability limit state was performed. For this purpose, it was assumed that the axial force of the cable is a random variable normally distributed. According to the results provided by Stromquist-LeVoir et al., it could be also assumed that this random variable has a range of variation of  $\pm 10\%$  [60]. A sample of stay cables with different values of the axial force was generated. The vibration serviceability limit state was assessed on this sample. For this purpose, the vibration serviceability limit state must be reformulated in order to take into account the uncertainty conditions. According to this, this limit state is met if a reliability index,  $\beta_s(\theta)$ , is greater than an allowable reliability index,  $\beta_t$ .

In order to compute the reliability index,  $\beta_s(\theta)$ , the maximum displacement of the stay cable (obtained from the different transient analyses performed on the sample of stay cables), which constitutes the demand of the wind action,  $D_a(\theta)$ , and the allowable displacement of the stay cable (established by the FHWA guidelines [6]), which constitutes the capacity of the structure,  $C_s$ , were determined. Additionally, as the wind action is defined according to a return period of 50 years, the corresponding value of the allowable reliability index is  $\beta_t = 1.35$ , according to the European guidelines [34].

As a numerical method in order to both determine the sample and compute the reliability index,  $\beta_s(\theta)$ , the Monte Carlo method was considered herein. A convergence analysis was performed to

determine the size of the sample [61]. As a result of this convergence analysis, the size of the sample was established at 100.

Finally, in order to evaluate the demand of the wind action,  $D_a(\theta)$ , the wind forces must be determined. For this purpose, simulations of the wind velocities were generated. The simulation of these wind velocities was addressed employing the wave superposition spectral-based method [8]. Both the von Karman spectra and a coherence function, as they are defined by the European guidelines [54], were employed herein. The following design parameters were considered for the wind simulation [54]: (i) basic wind velocity,  $v_{b,0} = 26$  m/s; (ii) a directional factor,  $c_{dir} = 1$ ; (iii) a season factor,  $c_{sea} = 1$ ; (iv) an orography factor,  $c_{oro} = 1$ ; (v) a terrain type III category (which involves a terrain factor,  $k_r = 0.216$ ; a roughness length,  $z_0 = 0.3$  m; and a minimum height,  $z_{min} = 5$  m); (vi) a duration of each simulation of 300 s; and (vii) a time step of  $5 \times 10^{-3}$  s [62]. In this study, the wind velocities were generated at ten different heights of the cable (resulting from dividing the cable into ten equal-length segments), as Figure 5 depicts. This mesh density was considered for all the simulations conducted in the paper, in order to ensure that all the obtained results were consistent. Although preliminary analyses performed by the authors concluded that the meshing in Figure 5 was adequate for our aims (illustrating the performance of the proposed motion-based approach), the reader should be aware of the fact that the numerical simulation of the structural response under wind excitation depends on such mesh density, so that further analyses are recommended. A graphical user interface [63] was developed in the commercial software Matlab [64] to evaluate the wind action following the above guidelines.

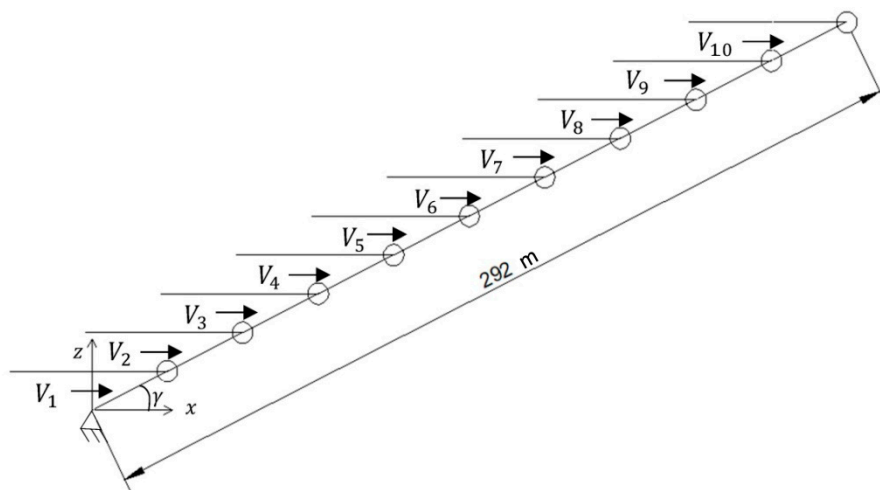


**Figure 5.** Representation of the ten different heights where the wind action is applied.

The application of Equations (11) and (12) allows the wind-induced forces in terms of the wind velocities to be computed. For this purpose, the following values for the characteristic parameters were adopted: (i) a density of the air,  $\rho = 1.23$  kg/m<sup>3</sup>; (ii) a drag coefficient,  $C_D = 1.2$  [2]; and (iii) a lift coefficient,  $C_L = 0.3$  [6].

Finally, a transient analysis (time history simulation) was performed for each element of the sample. The nonlinear geometrical behavior of the stay cables was considered for this analysis. A Newmark-beta method (an unconditionally stable method with parameters  $\beta_m = 1/4$  and  $\gamma_m = 1/2$ ) was considered to solve the transient analysis. Hence, the reliability index,  $\beta_s(\theta)$ , was computed from the results of this set of transient analysis. Subsequently, the vibration serviceability limit state of the stay cable under uncertainty conditions was assessed. Thus, the reliability index,  $\beta_s(\theta)$ , was lower than the allowable reliability index,  $\beta_t$ , so this limit state was not met.

In order to improve the dynamic behavior of this stay cables, different passive damping devices were installed at this stay cable. These passive damping devices were designed according to the proposed method. This design problem is described in next section.

### 4.3. Motion-Based Design of Passive Damping Devices under Uncertainty Conditions

Three different passive damping devices were considered for this study: (i) viscous damper; (ii) elastomeric damper; and (iii) friction damper. The FE method was employed to simulate the behavior of these damping devices. The software Ansys [57] was employed for this purpose. Figure 2 depicts the mechanical models, which simulate the behavior of each damper. For each passive damper, the following model was considered: (i) the viscous damper was modelled by a 1D element (COMBIN14) whose characteristic parameter was the damping coefficient,  $c_{d,v}$  [sN/m]; the elastomeric damper was also modelled by a 1D element (COMBIN14) whose characteristic parameters were the damping coefficient,  $c_{d,e}$  [sN/m], and the stiffness coefficient,  $k_{d,e}$  [N/m]; and (iii) the friction damper was modelled by a 1D element (COMBIN40) whose characteristic parameters were the damping coefficient,  $c_{d,f}$  [sN/m], the stiffness coefficient,  $k_{d,f}$  [N/m], and the friction force,  $f_f$  [N].

Consequently, the different dampers were implemented in the numerical model and designed according to the motion-based design method under uncertainty conditions. The three dampers were installed at a length of  $x_c = 0.03L$  according to the recommendations of Ref. [2]. The damper-cable interaction model is shown in Figure 2.

A search domain,  $[\theta_{\min}, \theta_{\max}]$ , for the characteristic parameters of the dampers was included in the optimization problem to ensure the physical meaning of the solutions obtained. The search domain was defined as follows: (i) the lower bound of the search domain,  $\theta_{\min}$ , was defined as  $\theta_{\min} = [c_{\min}, k_{\min}, f_{f_{\min}}]$  (where  $c_{\min}$  is the minimum value of the damping coefficient;  $k_{\min}$  is the minimum value of the stiffness coefficient, and  $f_{f_{\min}}$  is the minimum value of the friction force); and (ii) the upper bound of the search domain,  $\theta_{\max}$ , was defined as  $\theta_{\max} = [c_{\max}, k_{\max}, f_{f_{\max}}]$  (where  $c_{\max}$  is the maximum value of the damping coefficient;  $k_{\max}$  is the maximum value of the stiffness coefficient, and  $f_{f_{\max}}$  is the maximum value of the friction force).

The lower,  $c_{\min}$ , and upper,  $c_{\max}$ , bounds of the damping coefficient were determined considering both the requirement of the Scruton number [6] and the optimum damping coefficient of the Pacheco's universal curve [25]. According to this, the following bounds were established: (i)  $c_{\min} = 4.8 \times 10^4$  sN/m; and (ii)  $c_{\max} = 1.64 \times 10^5$  sN/m. This search range guarantees that any solution of this design problem avoids the occurrence of the rain–wind interaction phenomenon.

The search domain of the stiffness coefficient and the friction force were based on the results of previous research [2]. According to these results, the following bounds were established: (i) for the stiffness coefficient,  $k_{\min} = 5 \times 10^4$  N/m and  $k_{\max} = 5 \times 10^5$  N/m; and (ii) for the friction force,  $f_{f_{\min}} = 1 \times 10^4$  N and  $f_{f_{\max}} = 4 \times 10^4$  N.

In order to avoid falling into a local minimum, a global computational algorithm was considered for this optimization problem. Among the different computational algorithms, genetic algorithms were considered herein [65] for its simplicity and great efficiency to solve structural optimization problems.

Genetic algorithms are nature-inspired computational algorithms based on Darwin's natural selection theory. According to this, each possible value of the characteristic parameters of the damper is identified as a chromosome. Subsequently, each set of characteristic parameters is grouped into an individual (parameter vector). Later, the value of this parameter vector is improved via an iterative process where the value of the objective function is optimized. The optimization process can be summarized in the following steps: (i) an initial random population of parameter vectors is generated; (ii) the objective function is evaluated for all the individuals; (iii) a new population is created using three mechanisms (selection, crossover, and mutation); (iv) the objective function is evaluated for the individuals of the new population; (v) the steps (iii) and (iv) are repeated until some convergence criterion is met. The following parameters were considered for the considered genetic algorithms: (i) an initial population of 5 individuals; (ii) a crossover fraction of 0.4; (iii) a mutation fraction of 0.9; and (iv) a total number of iterations equal to 6.

As result of the optimization process, a Pareto front was obtained. Subsequently, a decision-making problem should be solved, the selection of the best solution among the different elements of the Pareto front. In order to address this problem, an additional condition was included. Among the

different elements of the Pareto front, the element of the Pareto front with a lower value of the damping coefficient was selected as best solution. The commercial software Ansys [57] and Matlab [64] were used to solve this design problem. The results of the optimization problem are summarized in the next sub-sections.

#### 4.3.1. Viscous Damper

First, the motion-based design of the viscous damper under uncertainty conditions was performed. The design problem of this viscous damper may be formulated as follows:

$$\begin{aligned} &\text{find } \theta = c_{d,v} \text{ to minimize } f(\theta) = c_{d,v} \\ &\text{subject to } \begin{cases} c_{\min} < c_{d,v} < c_{\max} \\ \beta_s(\theta) \geq \beta_t = 1.35. \end{cases} \end{aligned} \tag{21}$$

As result of the optimization process, the damping coefficient,  $c_{d,v}$ , was obtained. The optimum value obtained was  $c_{d,v} = 1.06 \times 10^5$  sN/m. The reliability index for this solution was,  $\beta_s(\theta) = 1.37$ , which met the design requirements. Figure 6 shows the maximum displacement at the mid-span of the cable damped by the viscous damper for the different elements of the sample.

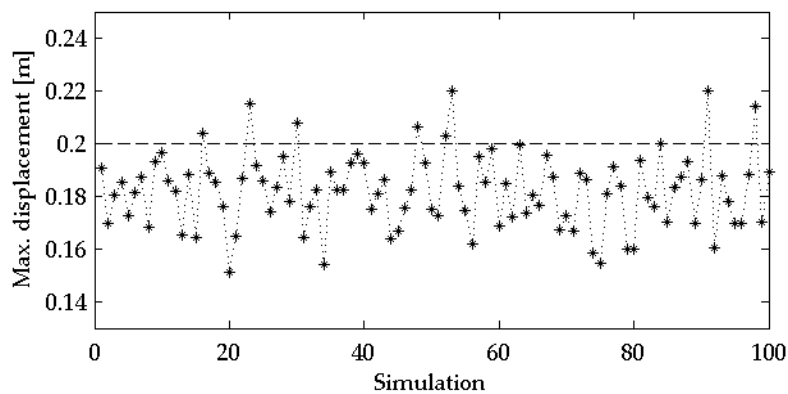


**Figure 6.** Maximum displacement at the mid-span of the stay cable damped by the viscous damper for the different elements of the sample.

#### 4.3.2. Elastomeric Damper

Subsequently, the motion-based design of the elastomeric damper under uncertainty conditions may be addressed. The design problem of this elastomeric damper may be defined as follows:

$$\begin{aligned} &\text{find } \theta = [c_{d,e}, k_{d,e}] \text{ to minimize } f(\theta) = [f_1, f_2] = [c_{d,e}, k_{d,e}] \\ &\text{subject to } \begin{cases} c_{\min} < c_{d,e} < c_{\max} \\ k_{\min} < k_{d,e} < k_{\max} \\ \beta_s(\theta) \geq \beta_t = 1.35. \end{cases} \end{aligned} \tag{22}$$

As result of the design process, the parameters of the elastomeric damper ( $c_{d,e}$  and  $k_{d,e}$ ) were obtained. The best solution among all the elements of the Pareto front was  $c_{d,e} = 1.22 \times 10^5$  sN/m and  $k_{d,e} = 1.30 \times 10^5$  N/m. The reliability index associated with this solution is,  $\beta_s(\theta) = 1.49$ , which met the design requirements. Figure 7 shows the maximum displacement at the mid-span of the cable damped by the elastomeric damper for the different elements of the sample.



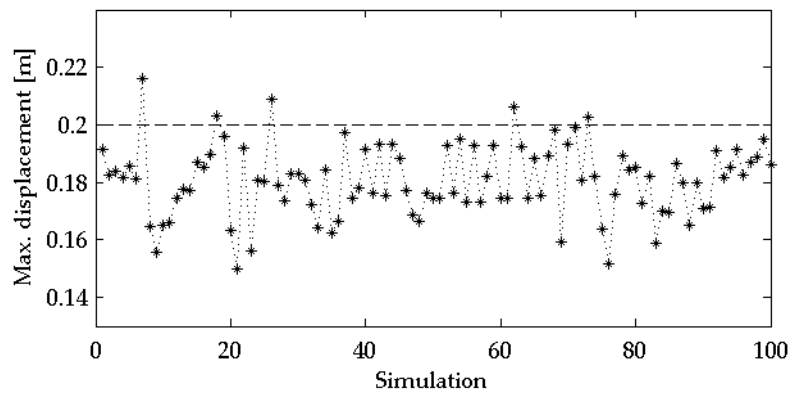


**Figure 7.** Maximum displacement at the mid-span of the stay cable with the elastomeric damper for the different elements of the sample.

### 4.3.3. Friction Damper

Finally, the motion-based design of the friction damper under uncertainty conditions was performed. The design problem of this friction damper may be formulated as follows:

$$\begin{aligned} \text{find } \theta = [c_{d,e}, k_{d,e}, f_f] \text{ to minimize } \mathbf{f}(\theta) = [f_1, f_2, f_3] = [c_{d,e}, k_{d,e}, f_f] \\ \text{subject to } \begin{cases} c_{\min} < c_{d,f} < c_{\max} \\ k_{\min} < k_{d,f} < k_{\max} \\ f_{f\min} < f_f < f_{f\max} \\ \beta_s(\theta) \geq \beta_t = 1.35. \end{cases} \end{aligned} \quad (23)$$

After the design process, the optimum value of the damping coefficient, stiffness coefficient, and friction force which characterize the friction damper were obtained. The optimum solution was  $c_{d,f} = 1.24 \times 10^5$  sN/m,  $k_{d,f} = 6.74 \times 10^4$  N/m and  $f_f = 2.95 \times 10^4$  N. The reliability index associated with this solution was  $\beta_s(\theta) = 1.55$ , which met the design requirements. Figure 8 shows the maximum displacement at the mid-span of the cable damped by the friction damper for the different elements of the sample.

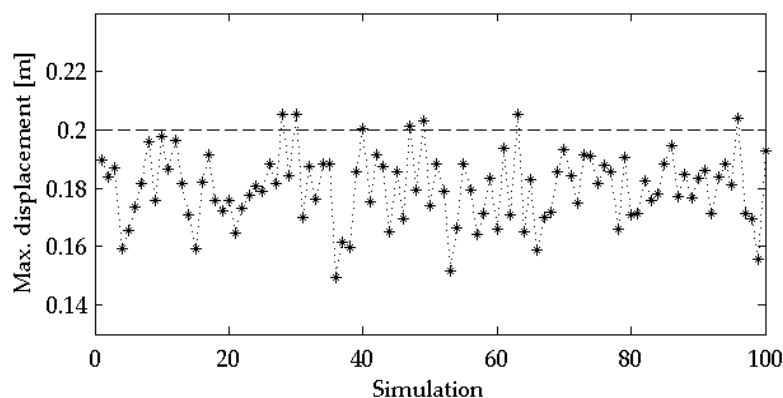


**Figure 8.** Maximum displacement at the mid-span of the stay cable damped by the friction damper for the different elements of the sample.

### 4.4. Discussion of Results

Finally, the performance of the proposed method was validated comparing the abovementioned results with the ones provided by a conventional one, the optimum damping coefficient of the Pacheco’s

universal curve [25]. This optimum value for a viscous damper can be determined using the following relationship:

$$c_{opt} = 0.10 \frac{mL\omega_1}{\frac{x_c}{L}}, \quad (24)$$

where  $\omega_1 = 2\pi f_1$  is the fundamental angular natural frequency of the stay cable [rad/s] and  $x_c$  is the distance between the anchorage of the cable and the point where the damper is implemented (Figure 2). As in the remaining cases, the viscous damper is located at the point,  $x_c = 0.03L$ , with respect to the lower anchorage. The optimum damping coefficient, according to this conventional method for the viscous damper was  $c_{opt} = 1.64 \times 10^3$  sN/m.

Thus, two main conclusions may be obtained via the comparison of the abovementioned results: (i) the motion-based design method under uncertainty conditions allows reduction of the characteristic parameter of the viscous damper by about 35% with respect to the conventional method; and (ii) for this case-study, the viscous damper appears to be the best choice to control the dynamic response of the longest cable of the Alamillo bridge, as a minimum value of the damping coefficient was obtained for this passive damper. The proposed method allows a better adjustment to the design requirements of the problem, reducing, as consequence, the size and the cost of the passive damping devices. Hence, the performance of the motion-based design method, for this particular problem, has been validated.

## 5. Conclusions

Stay cables are prone to vibrate under wind-induced vibrations, so that passive damping devices are usually employed to control their response. Nevertheless, the performance of these damping devices is directly affected by the sensitivity of the stay cables to both the variability of the external actions and the modification of the constitutive modal properties of the cables induced by the changes of the operational and environmental conditions. Accordingly, it is necessary to establish design methods which overcome these limitations and can be easily implemented for practical engineering applications.

For this purpose, a motion-based design method under uncertainty conditions was proposed and implemented herein. In this approach, the design problem is transformed into a constrained multi-objective optimization problem. Thus, the different components of the multi-objective function are defined in terms of the characteristic parameters of the considered passive damping device; and an inequality constraint is additionally included to guarantee an acceptable probability of failure of the structural system. As design criterion to evaluate the probability of failure, the compliance of the vibration serviceability limit state (according to the FHWA guidelines) was considered. Therefore, the computation of the probability of failure was performed via a reliability index. In this manner, the compliance of the vibration serviceability limit state is met if the reliability index is greater than an allowable value (according to the European guidelines). A sampling technique, the Monte Carlo method, was considered to determine numerically this index.

The performance of the method was validated numerically via its implementation for the design of three different passive damping devices (viscous, elastomeric, and friction dampers) when they are used to control the wind-induced vibrations of the longest stay cable of the Alamillo bridge (Seville). To this end, the effects of the rain-wind interaction phenomenon and the turbulent component of the wind action were considered as excitation sources. Additionally, and for comparison purposes, the passive damping devices were also designed according to a conventional method. As result of this study, a clear reduction of the values of the characteristic parameters of the dampers was obtained when the motion-based design method was applied, when compared to the results of the conventional method. Thus, the proposed method allows improvement of the design of passive damping devices for stay cables under wind-induced vibrations considering uncertainty conditions. This improvement is reflected in a reduction of both the size and the budget of the devices, which facilitates its installation. Nevertheless, despite the good performance of the proposed approach, further studies are recommended to validate experimentally the long-term behavior of passive damping devices designed according to this proposal.

**Author Contributions:** Conceptualization, J.N.-P. and J.F.J.-A.; Methodology, J.F.J.-A.; Programming, J.N.-P. and G.Q.; Software, J.N.-P. and G.Q.; Validation, J.F.J.-A. and I.M.D.; Writing—Original Draft Preparation, J.N.-P. and J.F.J.-A.; Writing—Review & Editing, J.F.J.-A.; Supervision, I.M.D. and A.S.; Funding Acquisition, I.M.D. All authors have read and agreed to the published version of the manuscript.

**Funding:** This work was partially funded by the Ministry of Science, Innovation and Universities (Government of Spain) under the Research Project SEED-SD (RTI2018-099639-B-I00). Additionally, the co-author, Javier Naranjo-Pérez, was supported by the research contract, USE-17047-G, provided by the Universidad de Sevilla.

**Conflicts of Interest:** The authors declare no conflict of interest.

## References

1. Abdel-Ghaffar, A.M.; Khalifa, M.A. Importance of Cable Vibration in Dynamics of Cable-Stayed Bridges. *J. Eng. Mech.* **1991**, *117*, 2571–2589. [[CrossRef](#)]
2. Caetano, E. *Cable Vibrations in Cable-Stayed Bridges*; IABSE: Zürich, Switzerland, 2007; Volume 9.
3. Lepidi, M.; Gattulli, V. Static and dynamic response of elastic suspended cables with thermal effects. *Int. J. Solids Struct.* **2012**, *49*, 1103–1116. [[CrossRef](#)]
4. Caetano, E.; Cunha, A.; Gattulli, V.; Lepidi, M. Cable–deck dynamic interactions at the International Gadiana Bridge: On-site measurements and finite element modelling. *Struct. Control Health Monit.* **2008**, *15*, 237–264. [[CrossRef](#)]
5. Domaneschi, M.; Martinelli, L. Extending the benchmark cable-stayed bridge for transverse response under seismic loading. *J. Bridge Eng.* **2013**, *19*, 04013003. [[CrossRef](#)]
6. *Wind-Induced Vibration of Stay Cables*; FHWA-HRT-05-083; Federal Highway Administration: New York, NY, USA, 2007.
7. Dyke, S.J.; Caicedo, J.M.; Turan, G.; Bergman, L.A.; Hague, S. Phase I benchmark control problem for seismic response of cable-stayed bridges. *J. Struct. Eng.* **2003**, *129*, 857–872. [[CrossRef](#)]
8. Cremona, C. *Comportement Au Vent Des Ponts*; Presses De L'école Nationale Des Ponts Et Chaussées; Association Française De Génie Civil: Paris, France, 2002.
9. Caracoglia, L.; Zuo, D. Effectiveness of cable networks of various configurations in suppressing stay-cable vibration. *Eng. Struct.* **2009**, *31*, 2851–2864. [[CrossRef](#)]
10. Bossens, F.; Preumont, A. Active tendon control of cable-stayed bridges: A large-scale demonstration. *Earthq. Eng. Struct. Dyn.* **2001**, *30*, 961–979. [[CrossRef](#)]
11. Johnson, E.A.; Baker, G.A.; Spencer, B.F., Jr.; Fujino, Y. Semiactive Damping of Stay Cables. *J. Eng. Mech.* **2007**, *133*, 1–11. [[CrossRef](#)]
12. Ali, H.-E.M.; Abdel-Ghaffar, A.M. Seismic Passive Control of Cable-Stayed Bridges. *Shock Vib.* **1995**, *2*, 918721. [[CrossRef](#)]
13. Rodellar, J.; Mañosa, V.; Monroy, C. An active tendon control scheme for cable-stayed bridges with model uncertainties and seismic excitation. *J. Struct. Control* **2002**, *9*, 75–94. [[CrossRef](#)]
14. Huang, P.; Wang, X.; Wen, Q.; Wang, W.; Sun, H. Active Control of Stay Cable Vibration Using a Giant Magnetostrictive Actuator. *J. Aerosp. Eng.* **2018**, *31*, 04018074. [[CrossRef](#)]
15. Zhou, H.J.; Sun, L.M. Damping of stay cable with passive-on magnetorheological dampers: A full-scale test. *Int. J. Civ. Eng.* **2013**, *11*, 154–159.
16. Chen, Z.H.; Lam, K.H.; Ni, Y.Q. Enhanced damping for bridge cables using a self-sensing MR damper. *Smart Mater. Struct.* **2016**, *25*, 085019. [[CrossRef](#)]
17. YeganehFallah, A.; Attari, N.K.A. Robust control of seismically excited cable stayed bridges with MR dampers. *Smart Mater. Struct.* **2017**, *26*, 035056. [[CrossRef](#)]
18. Zhao, Y.-L.; Xu, Z.-D.; Wang, C. Wind vibration control of stay cables using magnetorheological dampers under optimal equivalent control algorithm. *J. Sound Vib.* **2019**, *443*, 732–747. [[CrossRef](#)]
19. Xu, Y.L.; Zhou, H.J. Damping cable vibration for a cable-stayed bridge using adjustable fluid dampers. *J. Sound Vib.* **2007**, *306*, 349–360. [[CrossRef](#)]
20. Shi, X.; Zhu, S. Magnetic negative stiffness dampers. *Smart Mater. Struct.* **2015**, *24*, 072002. [[CrossRef](#)]
21. Zhou, P.; Fang, Q. Match of Negative Stiffness and Viscous Damping in A Passive Damper for Cable Vibration Control. Available online: <https://www.hindawi.com/journals/sv/2019/3208321/> (accessed on 30 September 2019).

22. Caracoglia, L.; Jones Nicholas, P. Passive hybrid technique for the vibration mitigation of systems of interconnected stays. *J. Sound Vib.* **2007**, *307*, 849–864. [[CrossRef](#)]
23. Jiménez-Alonso, J.F.; Sáez, A. Robust optimum design of tuned mass dampers to mitigate pedestrian-induced vibrations using multi-objective genetic algorithms. *Struct. Eng. Int.* **2017**, *27*, 492–501. [[CrossRef](#)]
24. Kovacs, I. Zur frage der seilschwingungen und der seildämpfung. *Bautechnik* **1982**, *59*, 325–332.
25. Pacheco, B.M.; Fujino, Y.; Sulekh, A. Estimation curve for modal damping in stay cables with viscous damper. *J. Struct. Eng.* **1993**, *119*, 1961–1979. [[CrossRef](#)]
26. Krenk, S. Vibrations of a taut cable with an external damper. *J. Appl. Mech.* **2000**, *67*, 772–776. [[CrossRef](#)]
27. Yoneda, M.; Maeda, K. A study on practical estimation method for structural damping of stay cables with dampers. *Doboku Gakkai Ronbunshu* **1989**, *1989*, 455–458. [[CrossRef](#)]
28. Ontiveros-Pérez, S.P.; Miguel, L.F.F.; Miguel, L.F.F. Robust Simultaneous Optimization of Friction Damper for the Passive Vibration Control in a Colombian Building. *Procedia Eng.* **2017**, *199*, 1743–1748. [[CrossRef](#)]
29. Connor, J.J. *Introduction to Structural Motion Control, MIT-Prentice Hall Series on Civil, Environmental and Systems Engineering*; Prentice Hall: Bergen, NJ, USA, 2003.
30. Naranjo-Pérez, J.; Jiménez-Manfredi, J.; Jiménez-Alonso, J.; Sáez, A. Motion-based design of passive damping devices to mitigate wind-induced vibrations in stay cables. *Vibration* **2018**, *1*, 269–289. [[CrossRef](#)]
31. Hao, P.; Wang, B.; Li, G.; Meng, Z.; Wang, L. Hybrid Framework for Reliability-Based Design Optimization of Imperfect Stiffened Shells. *AIAA J.* **2015**, *53*, 2878–2889. [[CrossRef](#)]
32. Wang, L.; Wang, X.; Li, Y.; Lin, G.; Qiu, Z. Structural time-dependent reliability assessment of the vibration active control system with unknown-but-bounded uncertainties. *Struct. Control Health Monit.* **2017**, *24*, e1965. [[CrossRef](#)]
33. Rathi, A.K.; Chakraborty, A. Reliability-based performance optimization of TMD for vibration control of structures with uncertainty in parameters and excitation. *Struct. Control Health Monit.* **2017**, *24*, e1857. [[CrossRef](#)]
34. *EN 1990 Eurocode 0: Basis of Structural Design*; European Committee for Standardization: Brussels, Belgium, 2005.
35. Wang, L.; Liu, J.; Yang, Y. A nonprobabilistic time-variant reliability-based optimization approach to the reliable active controller design of structural vibration considering convex uncertainties. *Struct. Control Health Monit.* **2018**, *25*, e2269. [[CrossRef](#)]
36. Binder, K.; Heermann, D. *Monte Carlo Simulation in Statistical Physics: An Introduction; Graduate Texts in Physics*, 5th ed.; Springer-Verlag: Berlin/Heidelberg, Germany, 2010; ISBN 978-3-642-03162-5.
37. Arora, J.S. *Optimization of Structural and Mechanical Systems*; World Scientific Publishing Co. Pte. Ltd.: 5 Toh Tuck Link, Singapore, 2007.
38. Nocedal, J.; Wright, S.J. *Numerical Optimization*; Springer Verlag: New York, NY, USA, 1999.
39. Holický, M. *Reliability Analysis for Structural Design*; African Sun Media: Stellenbosch, South Africa, 2009.
40. Warnitchai, P.; Fujino, Y.; Susumpow, T. A non-linear dynamic model for cables and its application to a cable structure system. *J. Sound Vib.* **1995**, *187*, 695–712. [[CrossRef](#)]
41. Caetano, E.; Cunha, A.; Taylor, C.A. Investigation of dynamic cable–deck interaction in a physical model of a cable-stayed bridge. Part I: Modal analysis. *Earthq. Eng. Struct. Dyn.* **2000**, *28*, 481–498. [[CrossRef](#)]
42. Johnson, E.A.; Christenson, R.E.; Spencer, B.F., Jr. Semiactive damping of cables with sag. *Comput. Aided Civ. Infrastruct. Eng.* **2003**, *18*, 132–146. [[CrossRef](#)]
43. Zhou, Q.; Nielsen, S.R.; Qu, W.L. Semiactive control of three-dimensional vibrations of an inclined sag cable with magnetorheological dampers. *J. Sound Vib.* **2006**, *296*, 1–22. [[CrossRef](#)]
44. Mehrabi, A.B.; Tabatabai, H. Unified finite difference formulation for free vibration of cables. *J. Struct. Eng.* **1998**, *124*, 1313–1322. [[CrossRef](#)]
45. Hoang, N.; Fujino, Y. Analytical study on bending effects in a stay cable with a damper. *J. Eng. Mech.* **2007**, *133*, 1241–1246. [[CrossRef](#)]
46. Yu, Z.; Xu, Y.L. Mitigation of three-dimensional vibration of inclined sag cable using discrete oil dampers—I. Formulation. *J. Sound Vib.* **1998**, *214*, 659–673. [[CrossRef](#)]
47. Connor, J.; Laflamme, S. Optimal Passive Damping Distribution. In *Structural Motion Engineering*; Springer: Berlin/Heidelberg, Germany, 2014; pp. 141–197.
48. Xu, Z.-D.; Shen, Y.-P.; Zhao, H.-T. A synthetic optimization analysis method on structures with viscoelastic dampers. *Soil Dyn. Earthq. Eng.* **2003**, *23*, 683–689. [[CrossRef](#)]

49. Zhou, H.; Sun, L.; Xing, F. Free vibration of taut cable with a damper and a spring. *Struct. Control Health Monit.* **2014**, *21*, 996–1014. [[CrossRef](#)]
50. Seong, J.-Y.; Min, K.-W. An analytical approach for design of a structure equipped with friction dampers. *Procedia Eng.* **2011**, *14*, 1245–1251. [[CrossRef](#)]
51. Hong, S. Time Domain Buffeting Analysis of Large-Span Cable-Stayed Bridge. Master's Thesis, FEUP. University of Porto, Porto, Portugal, 2009.
52. Solari, G. Gust-excited vibrations. In *Wind-Excited Vibrations of Structures*; Springer: Berlin/Heidelberg, Germany, 1994; pp. 195–291.
53. Davenport, A.G. The Dependence of Wind Loads on Meteorological Parameter. *Wind Eff. Build. Struct.* **1968**, *1*, 19–82.
54. EN 1991-1-4 Eurocode 1. Actions on Structures—Part 1-4: General Actions—Wind Actions; European Committee for Standardization: Brussels, Belgium, 2005.
55. Casas, J.R.; Aparicio, A.C. Monitoring of the Alamillo cable-stayed bridge during construction. *Exp. Mech.* **1998**, *38*, 24–28. [[CrossRef](#)]
56. Casas, J.R.; Aparicio, A.C. Rain-wind-induced cable vibrations in the Alamillo cable-stayed bridge (Sevilla, Spain). Assessment and remedial action. *Struct. Infrastruct. Eng.* **2010**, *6*, 549–556. [[CrossRef](#)]
57. Ansys Mechanical 19.0. Ansys Inc. 2019. Available online: <http://www.ansys.com/> (accessed on 1 October 2019).
58. Simiu, E.; Scanlan, R.H. *Wind Effects on Structures: Fundamentals and Applications to Design*, 3rd ed.; John Wiley & Sons, Inc.: New York, NY, USA, 1996.
59. EN 1993-1-11 Eurocode 3: Design of Steel Structures-Part 1-11: Design of Structures with Tension Components; European Committee for Standardization: Brussels, Belgium, 2006.
60. Stromquist-LeVoi, G.; McMullen, K.F.; Zaghi, A.E.; Christenson, R. Determining Time Variation of Cable Tension Forces in Suspended Bridges Using Time-Frequency Analysis. *Adv. Civ. Eng.* **2018**, *2018*. [[CrossRef](#)]
61. Naranjo-Pérez, J.; Jiménez-Alonso, J.F.; Díaz, I.M.; Sáez, A. Motion-based design of viscous dampers for cable-stayed bridges under uncertainty conditions. In Proceedings of the 5th International Conference on Mechanical Models in Structural Engineering, CMMoST 2019, Alicante, Spain, 23–25 October 2019.
62. Park, S.; Bosch, H.R. *Mitigation of Wind-Induced Vibration of Stay Cables: Numerical Simulations and Evaluations*; Federal Highway Administration: Hampton, VA, USA, 2014.
63. Jurado, D. Simulación Estocástica De Cargas Para Análisis Dinámico De Estructuras En Ingeniería Civil. Master's Thesis, Universidad de Sevilla, Seville, Spain, 2017.
64. Matlab Inc. Matlab R2019b. Available online: <http://www.mathworks.com/> (accessed on 15 October 2019).
65. Koh, C.G.; Perry, M.J. *Structural Identification and Damage Detection Using Genetic Algorithms: Structures and Infrastructures Book Series*; CRC Press: Boca Raton, FL, USA, 2017; Volume 6.

